ACS OMEGA

Open Access

http://pubs.acs.org/journal/acsodf

Article

Structural, Optical, and Magnetic Properties of Pure and Ni–Fe-Codoped Zinc Oxide Nanoparticles Synthesized by a Sol–Gel Autocombustion Method

Nasar Ahmed, Zakia Khalil, Zahid Farooq, Khizar-ul-Haq, Shabnam Shahida, Ramiza, Pervaiz Ahmad, Karwan Wasman Qadir,* Rajwali Khan, and Qayyum Zafar*

Cite This: *ACS Omega* 2024, 9, 137–145

Read Online

ACCESS | Metrics & More | Article Recommendations

ABSTRACT: Pure and Ni–Fe-codoped $Zn_{1-2x}Ni_xFe_xO$ (x = 0.01, 0.02, 0.03, and 0.04) nanoparticles were effectively synthesized using a sol–gel autocombustion procedure. The structural, optical, morphological, and magnetic properties were determined by using X-ray diffraction (XRD), ultraviolet–visible (UV–vis), scanning electron microscopy, and vibrating sample magnetometer techniques. The XRD confirmed the purity of the hexagonal wurtzite crystal structure. XRD analysis further indicated that Fe and Ni successfully substituted the lattice site of Zn and generated a single-phase $Zn_{1-2x}Ni_xFe_xO$ magnetic oxide. In addition, a significant morphological change was observed with an increase in the dopant concentration by using high-resolution scanning electron microscopy. The UV–vis spectroscopy analysis indicated the redshift in the optical band gap with increasing dopant concentration signifying a progressive decrease in the optical band gap. The vibrating sample magnetometer analysis revealed that the doped samples exhibited ferromagnetic properties at room temperature with an increase in the dopant concentration. Dopant concentration was confirmed by using energy-dispersive X-ray spectroscopy. The current results provide a vital method to improve the magnetic properties of ZnO nanoparticles, which may get significant attention from researchers in the field of magnetic semiconductors.

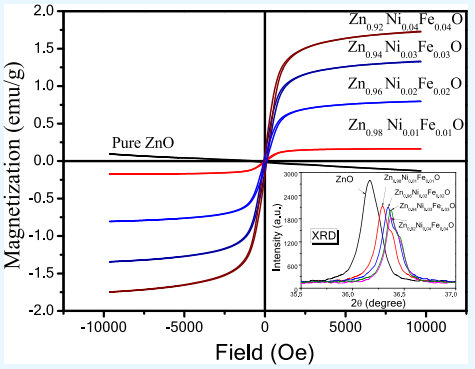

1. INTRODUCTION

Due to exceptional physical and chemical properties, nanomaterials have recently received substantial attention in various fields of fundamental and applied research. Among other nanomaterials, ZnO has specifically received momentous attention for a couple of years due to its unique characteristics. Major properties that distinguish ZnO among others are the wide and direct band gap of 3.39 eV and its piezoelectricity.[1] Due to these remarkable properties, it has several applications in different fields such as optoelectronics,[1] electromechanical devices,[2] light-emitting diodes,[3] photocatalysis,[4] piezoelectricity,[5] nanogenerators,[6] solar cells,[7] smart windows,[8] transistors,[9] gas sensors,[10] and much more.[1−3] It is a multifunctional semiconductor that can also be used as a magnetic storage device or optical/electrical switching device.[1,6−10] ZnO is low cost, abundant, biosafe, and biocompatible, thereby it is used in various medical applications.[11] Interestingly, the optical and electrical properties of ZnO can be easily tuned by transition metal doping and specifically by varying the dopant concentrations. As a result, doped ZnO nanoparticles (NPs) have gained huge interest in the past decade.[4−12] Significantly improved magnetic, electrical, optical, and structural properties have been reported by many researchers.[9−12] Fabrication of transition metal-doped ZnO can be achieved by several different techniques,[1−5] microemulsion process,[7−10] microwave hydrothermal process,[12] sol–gel synthesis,[13] precipitation method,[14] chemical vapor,[15] solvothermal synthesis,[12,13] chemical method,[1,13] and autocombustion method.[13] The autocombustion method, however, is a short, time-saving, and homogeneous method.

It is well established from previous research that NPs of ZnO have diamagnetic properties,[1,16] which is also confirmed by our results. Diluted magnetic semiconductors involve incorporating transition metal ions into the host lattice of semiconductors.[17] Due to their potential to be turned into a new class of spintronic devices such as logic devices,[18] spin-valve transistors,[19] and spin light-emitting diodes,[20] and due to room temperature ferromagnetic behavior, diluted magnetic

Received: March 14, 2023
Accepted: October 9, 2023
Published: December 19, 2023

semiconductors have gained a lot of interest in recent years.[21] Predictions were made by theoretical studies that the transition metal-doped ZnO is the most suitable kind of candidate for room temperature ferromagnetism[22−26] since 3d transition metals (Co, Ni, Fe, Mn, Cu, V, etc.)-doped semiconductor-based magnetic semiconductors reveal ferromagnetic behavior above room temperature as well.[23] The room temperature ferromagnetism was discovered in Fe-doped ZnO nanocrystals made using the sol−gel process, and it was determined that this is how ferromagnetism is thought to have originated rather than through secondary phases like iron oxides.[24] Weak room temperature ferromagnetism was found in coprecipitation-produced Fe-doped ZnO nanorods.[25] The ZnO:Ni grown through a simple coprecipitation technique was also found to have room temperature ferromagnetism behavior.[26] Codoping in ZnO with the transition metals showed ferromagnetism.[27] Laiho et al. observed the intrinsic ferromagnetism in Fe- and Mg-codoped ZnO.[28] Similarly, room temperature ferromagnetic 2% Ni-doped ZnO rods were synthesized by high pulsed magnetic field-assisted hydrothermal method.[29] Wu et al. utilized the hydrothermal approach to fabricate the codoped ZnO nanorods, and it was observed that Ni−Fe-codoped ZnO has higher room temperature ferromagnetism as compared to single-element-doped ZnO.[30] From these investigations, it was observed that the fabrication technique plays a vital role in the room temperature ferromagnetic behavior of ZnO, and codoping (Ni−Fe) can be an effective way to improve the ferromagnetic ordering in ZnO systems.

In the present contribution, the synthesis of Ni- and Fe-codoped zinc oxide was achieved using the autocombustion method because of its simplicity and cost-effectiveness. The effect of doping on different properties of transition metal-doped zinc oxide is investigated. It was observed that the behavior of doped NPs can be tuned from diamagnetism to paramagnetism by increasing the doping concentrations. Current research work demonstrates that the autocombustion method is an active method to get good-quality magnetic materials in a very short period.

2. EXPERIMENTAL DETAILS

In this work, $Zn_{1-2x}Ni_xFe_xO$ (x = 0.01, 0.02, 0.03, and 0.04) NPs were synthesized by a simple and low-temperature autocombustion procedure. Pure ZnO NPs were synthesized using the autocombustion method as discussed in our previous article.[15] In brief, $Zn(NO_3)_2{\cdot}6H_2O$ and glycine were mixed in distilled water, and the whole mixture was transferred on a hot plate (Robus Technology RT-550) at 300 °C under constant stirring (fixed at 550 rpm) for one and half hours. Subsequently, the solution was converted into a gel. After a few minutes, combustion was started and a large amount of volatile gases evolved during the combustion, and an off-white color powder of ZnO was obtained. Then, samples were dried and ground in an agate mortar to get fine particles.

2.1. Fabrication of Ni−Fe-Codoped ZnO NPs. Fe- and Ni-doped ZnO NPs were fabricated by taking the appropriate amount of zinc nitrate $Zn(NO_3)_2{\cdot}6H_2O$, glycine, iron nitrate $Fe(NO_3)_2{\cdot}6H_2O$, and nickel nitrate $Ni(NO_3)_2{\cdot}6H_2O$. These materials were measured by a highly sensitive electronic balance (AFD AK-300H). These materials were mixed in distilled water (100 mL) and placed on the magnetic stirrer plate. The mixed solution was then transferred to a hot plate, which was adjusted at 300°C for 1.5 h. After 1 h, a dark color gel was obtained, and after 1.5 h, combustion was initiated. During the combustion process, gases escaped and fine powder was collected at the bottom. To remove the volatile gases from the samples, all the samples were calcined in the Muffle furnace at 500 °C for 3 h. The experimental procedure used in this article is also discussed in our previous work.[15] It is pertinent to mention that an agate mortar was utilized to get finely ground powder of doped and undoped NPs. The resulting samples were characterized by various instrumental techniques such as X-ray diffraction (XRD), scanning electron microscopy (SEM), Fourier transform infrared spectroscopy (FTIR), and vibrating sample magnetometer (VSM). The crystal structure, crystalline quality, and average crystallite size of the particles were determined by XRD (Bruker B8 advance) using graphite-filtered CuKα radiation (λ = 1.54056 Å). The surface morphology was investigated by using a scanning electron microscope (JSM-5910). Determination of energy band gap and absorption coefficient was performed by diffuse reflectance UV−vis (PerkinElmer UV/vis/NIR spectrometer Lambda 950), and the presence of functional groups was detected through FTIR of powder samples. The magnetic measurements were performed on a VSM (Lake Shore 7407) operated under an applied field of 10k Oe to study the magnetic properties of the samples.

3. RESULTS AND DISCUSSION

3.1. XRD Analysis. The powder samples were characterized by XRD and the diffraction patterns of pure ZnO and $Zn_{1-2x}Ni_xFe_xO$ (x = 0.01, 0.02, 0.03, and 0.04) are shown in Figure 1.

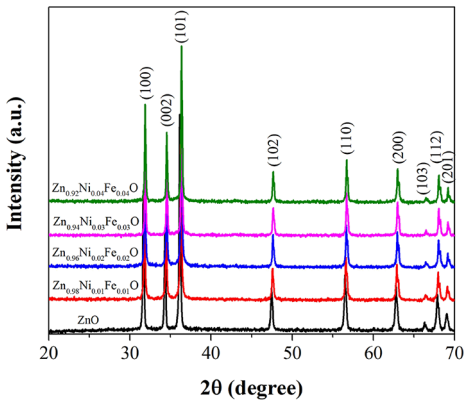

Figure 1. XRD patterns of all pure and doped ZnO NPs calcined at 500 °C.

The XRD patterns showed good matching with the hexagonal P63mc structure of ZnO index (JCPDS) No. 01-1136. It is clear from the XRD pattern that all the characteristic diffraction peaks for (100), (002), (101), (102), (110), (200), (103), (112), and (201) planes confirmed the formation of the hexagonal wurtzite structure.[12,13,30] No impurities or secondary phases of any materials were observed. It is also clear from Figure 1 that the position of the most significant peak (101) shifts toward a higher angle and intensity decreases with an increase in the dopant concentration. The crystallinity of wurtzite zinc oxide is reduced by the addition of Ni and Fe dopant atoms. A decrease in the lattice parameter is another indication of the successful substitution of both the Ni and Fe atoms at the Zn site. In addition, Figure 2 shows that by increasing the doping concentration of Ni and Fe in ZnO, the

https://doi.org/10.1021/acsomega.3c01727
ACS Omega 2024, 9, 137−145

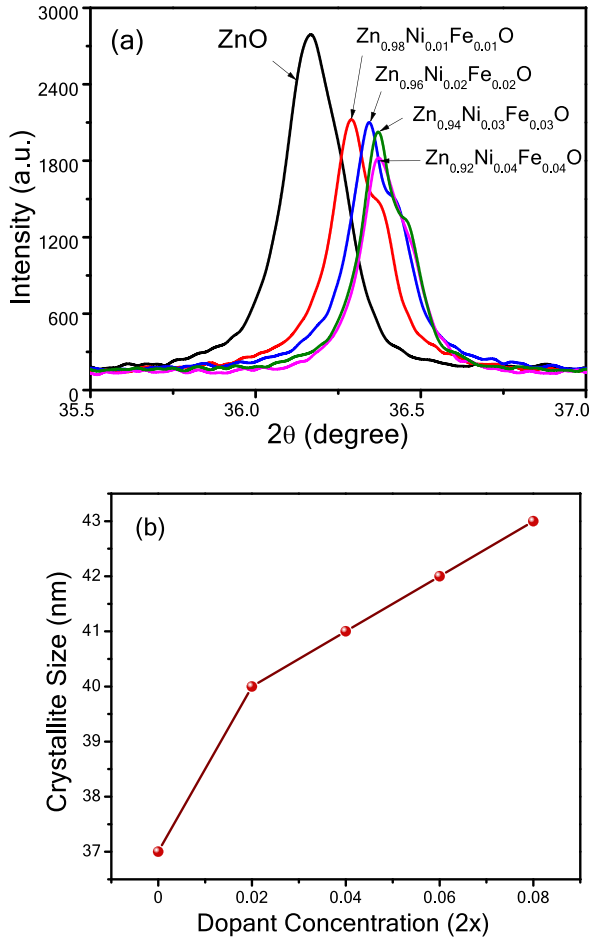

Figure 2. (a) Shift and reduction in the intensity of (101) peak with increasing dopant concentration and (b) change in crystallite size with increasing dopant concentration.

(101) peak shifts toward the higher angle and intensity was reduced, which shows a reduction in the crystallinity of doped ZnO NPs. Variation in crystallite size by doping Ni and Fe at different concentrations is shown in Figure 2b.

It was observed that the crystallite size increased with an increase in the dopant concentrations. As the wurtzite ZnO has many native defects due to the lattice structure that contains large voids, it can easily be filled by several atoms. In Figure 2a, a shoulder peak at the right side may also be observed in doped samples, which confirms the secondary phases of iron oxide (Fe_2O_3) in the rhombohedral crystalline phase of hematite (standard card PDF 01-087-1165). In the previous studies, the same behavior of secondary phase presence was observed, and it is believed that the formation of secondary phase in the final product may be related to the large quantities of gases formed during combustion explosions.[31−33]

Figure 2b and Table 1 show that the crystallite size specifically increases from 37 to 43 nm with an increase in Ni−Fe concentration from 0 to 4%. The average crystallite size was calculated using Scherer's formula. The inclusion of Fe into $Zn_{1-2x}Ni_xO$ (x = 0.01, 0.02, 0.03, and 0.04) diminishes the intensity of all the peaks and shifts the peak position which may be due to the disorder or defects generated by the addition of Fe^{2+} ions in Zn−Ni−O sites. It is well-known that the radius of Fe^{2+} ions is larger than that of Zn^{2+} and Fe^{3+} individually.[30,31] Table 1 shows that crystallite size was enhanced by simultaneous doping of Fe into Zn−Ni−O due to the replacement of Fe^{2+} instead of Zn^{2+}, and similar behavior was also observed by many authors.[13,17,22,26,29−34] The lattice parameters ($a = b$) of $Zn_{1-2x}Ni_xFe_xO$ (x = 0.01, 0.02, 0.03, and 0.04) measured from XRD data varied from 3.2413 to 3.2357 Å and parameter c from 5.1903 to 5.1813 Å. These values are slightly less than that of zinc oxide having lattice parameters $a = b$ = 3.2478 and c = 5.2034 Å. The decrease in lattice parameters revealed that the doping of Ni and Fe in ZnO does not change the wurtzite crystal structure of zinc oxide, causing a reduction in peak intensity. It also reveals the successful substitution of Ni and Fe at the Zn sites. The results indicate that all Fe and Ni ions are incorporated into the lattice of the host ZnO crystal.[21]

3.2. Morphological Studies Using SEM. The morphologies of pure and doped ZnO samples were studied by using a scanning electron microscope operated at 15 kV. Figure 3a shows the morphology of pure ZnO samples at ×30,000 magnification. The SEM images of pure and doped zinc oxide samples calcined at 500 °C revealed that grains are almost hexagonal in shape, and agglomeration of particles has occurred. SEM micrographs of $Zn_{0.98}Ni_{0.01}Fe_{0.01}O$, $Zn_{0.96}Ni_{0.02}Fe_{0.02}O$, $Zn_{0.94}Ni_{0.03}Fe_{0.03}O$, and $Zn_{0.92}Ni_{0.04}Fe_{0.04}O$ samples at ×30,000 magnifications are also shown in Figure 3b−e. These results showed that the particle size of hexagonal nanostructures increased with doping concentration. SEM images were taken for all of the samples at the same magnification, and it was observed that grains are almost hexagonal in shape, and agglomeration of the particles is observed, which may be due to the higher flame temperature of glycine. Results obtained using SEM images also support the XRD results.

To confirm the concentration of prepared samples, compositional analysis was carried out using the energy-dispersive X-ray spectroscopy (EDX) technique. Figure 4a−d represents the EDX spectra of $Zn_{0.98}$ $Ni_{0.01}$ $Fe_{0.01}O$, $Zn_{0.968}Ni_{0.02}Fe_{0.02}O$, $Zn_{0.94}Ni_{0.03}Fe_{0.03}O$, and $Zn_{0.92}Ni_{0.04}Fe_{0.04}O$ NPs. EDX spectra confirmed the elemental composition of the prepared samples. For Zn, sharp EDX peaks arise around 1.1 and 8.9 keV, for Fe at 0.5, 6.5, and 8.9 keV, and for Ni peaks at 1, 7.4, and around 8 keV. It can be seen that samples consist of oxygen and zinc mostly. No extra impurity element occurrence

Table 1. Estimation of the Crystallite Size, Unit Cell Volume, Lattice Parameters, Full Width at Half-Maximum, and Corresponding Angles for Pure and Doped ZnO

sample	angle (2θ)°	full width at half-maximum (deg)	$a = b$ (Å)	c (Å)	unit cell volume (Å)	crystallite size (nm)
ZnO	36.17	0.2162	3.2478	5.2034	47.55	37
$Zn_{0.98}Ni_{0.01}Fe_{0.01}O$	36.30	0.1993	3.2413	5.1903	47.34	40
$Zn_{0.96}Ni_{0.02}Fe_{0.02}O$	36.34	0.1935	3.2367	5.1844	47.22	41
$Zn_{0.94}Ni_{0.03}Fe_{0.03}O$	36.36	0.1899	3.2357	5.1813	47.17	42
$Zn_{0.92}Ni_{0.04}Fe_{0.04}O$	36.38	0.1834	3.2352	5.1813	47.16	43

https://doi.org/10.1021/acsomega.3c01727
ACS Omega 2024, 9, 137−145

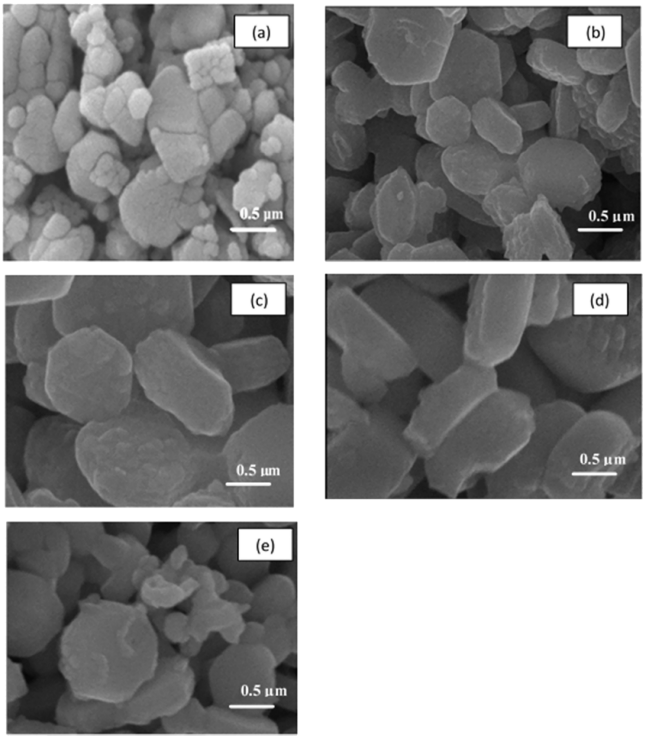

Figure 3. SEM micrographs of (a) pure ZnO, (b) $Zn_{0.98}Ni_{0.01}Fe_{0.01}O$, (c) $Zn_{0.96}Ni_{0.02}Fe_{0.02}O$, (d) $Zn_{0.94}Ni_{0.03}Fe_{0.03}O$, and (e) $Zn_{0.92}Ni_{0.04}Fe_{0.04}O$ at ×30,000 magnification.

was seen. The actual weight percentages of dopant elements were confirmed by using EDS results.

3.3. Optical Characteristics. Undoped, Ni- and Fe-codoped ZnO NPs prepared by the sol−gel autocombustion technique were used for the optical studies. The optical properties of the synthesized sample were measured by using diffuse reflectance spectroscopy (DRS) between the wavelengths of 250 and 800 nm. The diffuse reflectance spectra of all synthesized samples (at room temperature) are shown in Figure 5. The DRS of pure ZnO shows a sharp fall in

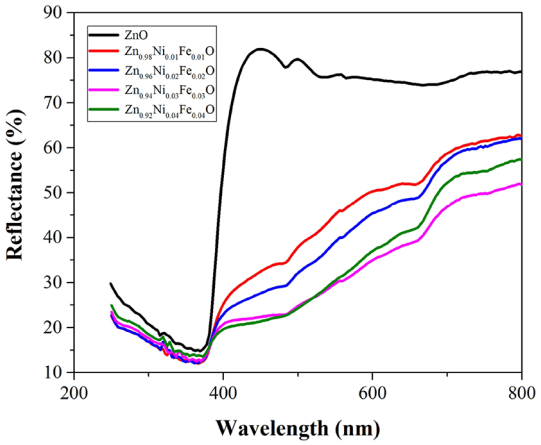

Figure 5. Diffuse reflectance spectra of pure and Ni−Fe-codoped ZnO samples.

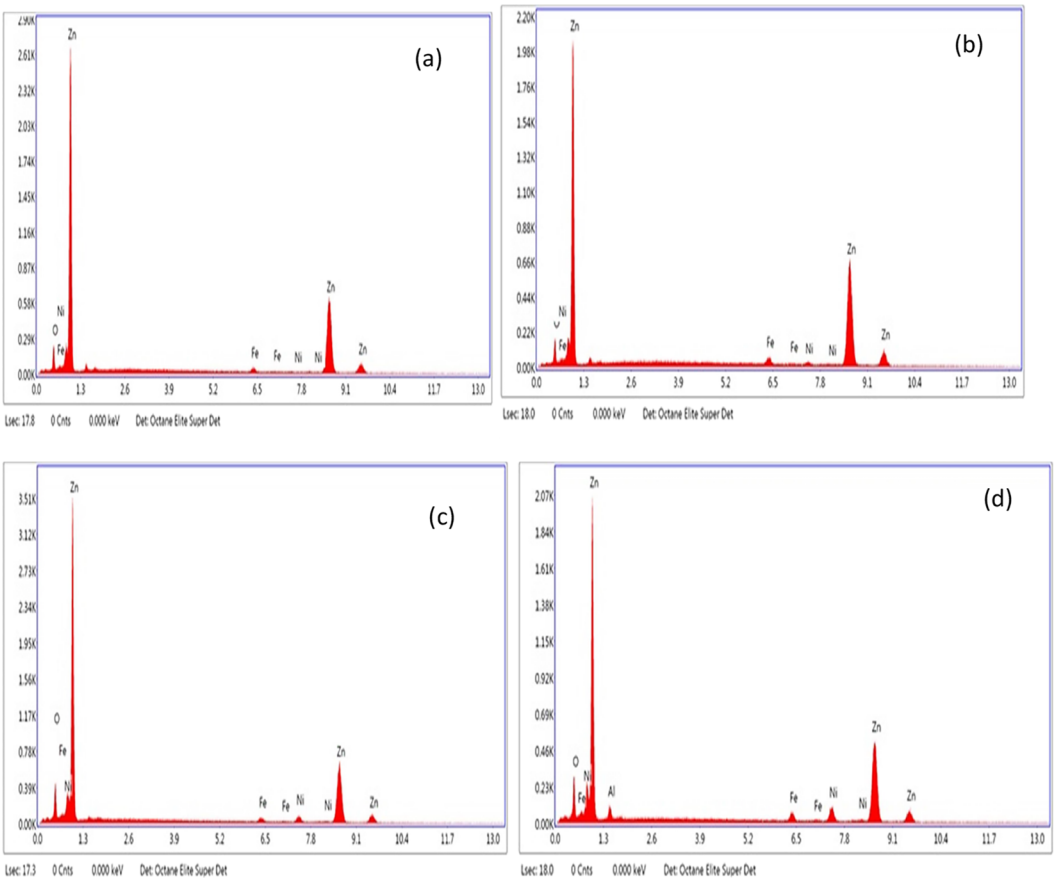

Figure 4. EDX spectra of (a) $Zn_{0.98}Ni_{0.01}Fe_{0.01}O$, (b) $Zn_{0.96}Ni_{0.02}Fe_{0.02}O$, (c) $Zn_{0.94}Ni_{0.03}Fe_{0.03}O$, and (d) $Zn_{0.92}Ni_{0.04}Fe_{0.04}O$ NPs.

https://doi.org/10.1021/acsomega.3c01727
ACS Omega 2024, 9, 137−145

reflectance, corresponding to the absorption edge with maximum transparency in the visible region. All doped samples demonstrate a reduction in percent reflectance than pure ZnO showing overwhelming band gap excitations in the visible region.[22−24]

The significance of this effect is more visible after the application of the Kubelka−Munk function. From diffuse reflectance spectroscopy, the absorbance is calculated using the Kubelka−Munk equation

$$F(R) = \frac{1 - R^2}{2R} \quad (1)$$

where $F(R)$ is the Kubelka−Munk function, and R is the reflectance. The optical band gap was calculated from DRS by plotting $h\nu$ along the x-axis and $[F(R)h\nu]^2$ along the y-axis. The linear region of these plots was extrapolated to $(F(R)h\nu)^2 = 0$ to obtain the values of the direct band gaps.[35] The variation in band gaps of NPs with the doping concentration may be due to different crystal defects in ZnO crystal.[36,37] Figure 6a shows the energy band gap of the pure ZnO sample

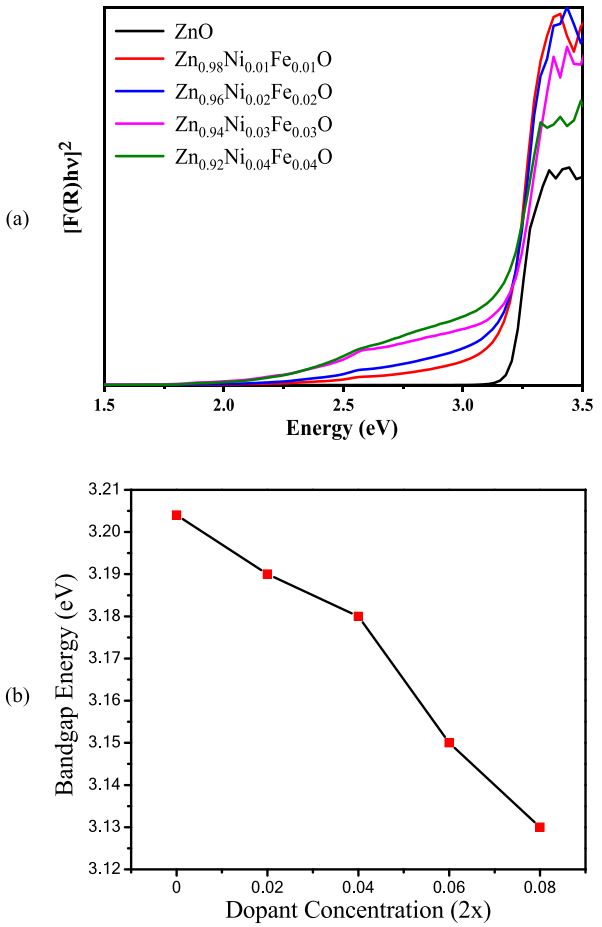

Figure 6. (a) Tauc plots of $[F(R)h\nu]^2$ vs energy for all the samples. (b) Variation of band gap with doping concentration.

and codoped sample calcined at 500 °C. It can be observed that the energy band gap (E_g) of pure ZnO is 3.204 eV, and a decrease in the band gap with increasing dopant concentration was observed which is attributed to the defect chemistry variation in the doped sample.[36]

Table 2 shows the values of band gap (E_g) of pure and codoped ZnO NPs using the Tauc plot. The values of band

Table 2. Values of Energy Band Gap (E_g) of Pure and Codoped ZnO NPs

sample	band gap (eV)
ZnO	3.20
$Zn_{0.98}Ni_{0.01}Fe_{0.01}O$	3.19
$Zn_{0.96}Ni_{0.02}Fe_{0.02}O$	3.18
$Zn_{0.94}Ni_{0.03}Fe_{0.03}O$	3.15
$Zn_{0.92}Ni_{0.04}Fe_{0.04}O$	3.13

gaps progressively decreased from 3.20 to 3.13 eV with increasing doping concentrations of Ni and Fe. Figure 6b shows the variation of the band gap with dopant concentration, which is in good agreement with the result reported by many authors.[38,39] According to Wu et al., the sp-d spin-exchange interactions between the band electrons and the localized d electrons of the transition metal ions substituting the cation, generally result in a decrease in the band gap in transition metal-doped II−VI semiconductors.[39]

Accordingly, in our synthesized samples, when we add Ni and Fe in ZnO, the s-d and p-d exchange interactions between the localized d electrons of Fe and Ni and the band electrons of ZnO may change the energy band structure, which results in the reduction of the band gap. The reduction of the band gap toward the visible range is expected to be helpful for applications in photocatalysis reactions and solar cell devices due to the absorption of more solar energy in the visible spectrum.

Figure 7a shows the variation of band gap energy with the crystallite size, and it was observed that the energy band gap showed a decreasing trend with the increase in the crystallite size of codoped ZnO NPs, a similar trend that has also been reported by various authors.[34,36−38] It is believed that the number of atoms that form the crystallite size increases. This as a result renders the valence and conduction electrons more attractive to the ion core of the particles and hence results in a reduction of the band gap of the particles.[39,40] The relationship between the band gap and the refractive index of the material is of high interest because such evaluations lead to multiple applications. Band gap and refractive index of semiconductors represent two key physical perspectives that illustrate their electronic and optical properties. In 1950, Moss presented a basic relationship between these two properties[41]

$$n^4 E_g = 95 \text{ eV} \quad (2)$$

The refractive index in semiconductors is the measure of its transparency to incident spectral radiations. The threshold for the absorption of a photon in a semiconductor is determined by the energy gap. This information is very useful for a wide range of audiences because pre-knowledge of band gap and refractive index is required for devices such as photonic crystals, detectors, and waveguides. Figure 7b shows that with an increase in the band gap, refractive index and polarizability decreased, which was observed by many authors.[38−40,42,43] It is also observed that with increasing doping concentrations of Ni and Fe, the band gap decreased and the refractive index increased from 2.334 to 2.347.

3.4. Fourier Transform Infrared Spectroscopy. FTIR is one of the most extensively used techniques for detecting functional groups in pure compounds and mixtures. The FTIR spectra of pure and doped ZnO NPs prepared using the sol−gel combustion method and calcined at 500 °C have been studied. Similar absorption bands were observed in the doped

https://doi.org/10.1021/acsomega.3c01727
ACS Omega 2024, 9, 137−145

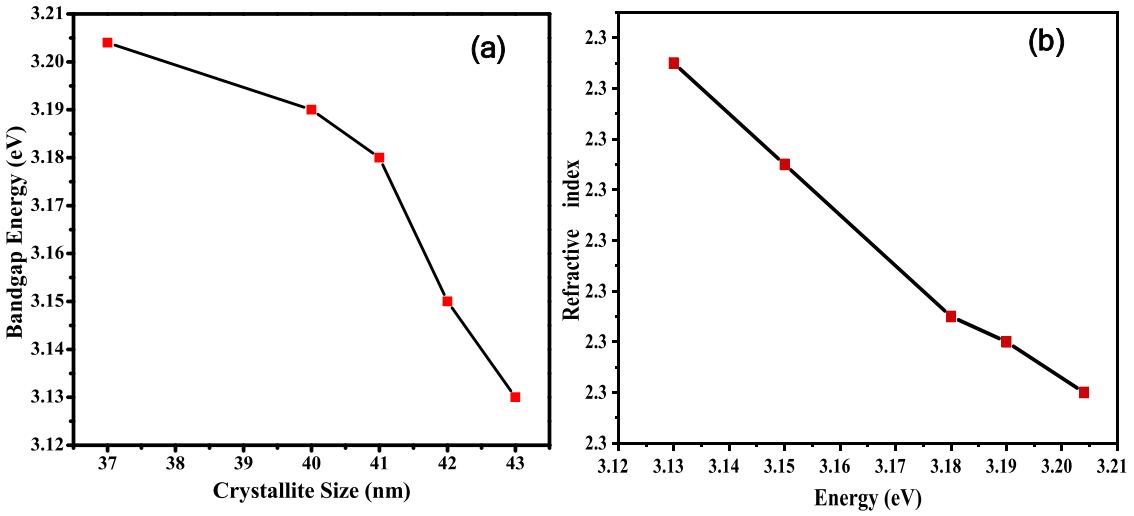

Figure 7. (a) Variation of band gap with crystallite size and (b) variation of refractive index with energy band gap (eV).

samples. Therefore, in Figure 8, we present the results of pure ZnO and $Zn_{0.98}Ni_{0.01}Fe_{0.01}O$ NPs for the comparison of pure and doped ZnO.

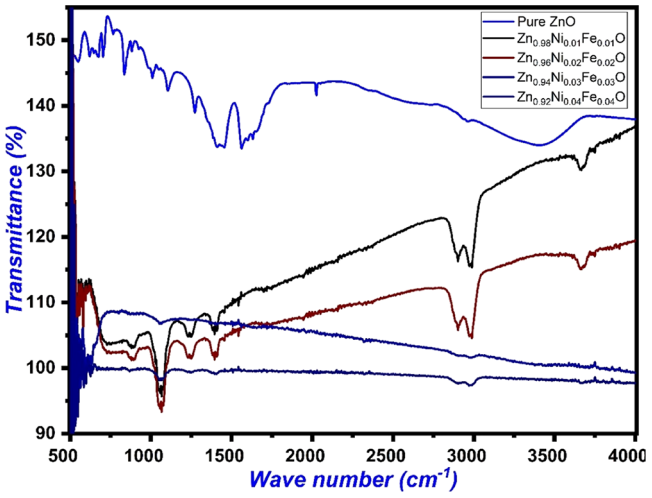

Figure 8. FTIR spectra of pure and pure and Ni−Fe-codoped ZnO samples.

The absorption bands around ~2900 cm^{-1} are related to the C−H mode. The peaks lying from ~1500 to ~1700 cm^{-1} represent the functional group corresponding to the C−O symmetric and antisymmetric stretching modes. In the spectra, the main absorption between 700 and 1000 cm^{-1} represents the stretching mode of Zn−O in pure ZnO, and it shows characteristic absorption bands due to the influence of doping.[44] The medium bands below 1000 cm^{-1} are assigned to the vibrational frequencies resulting from changes in the microstructural features caused by the addition of Ni and Fe to the Zn−O lattice. The results obtained from FT-IR spectra of pure ZnO and $Zn_{0.98}Ni_{0.01}Fe_{0.01}O$ NPs confirm the formation of ZnO NPs.

3.5. Magnetic Characterization. The magnetic nature of transition metal-doped materials was investigated by using the VSM at room temperature. The magnetization measurements were performed by cycling the field between ±10,000 Oe. Figure 9 shows the magnetic hysteresis ($M-H$) curves of the

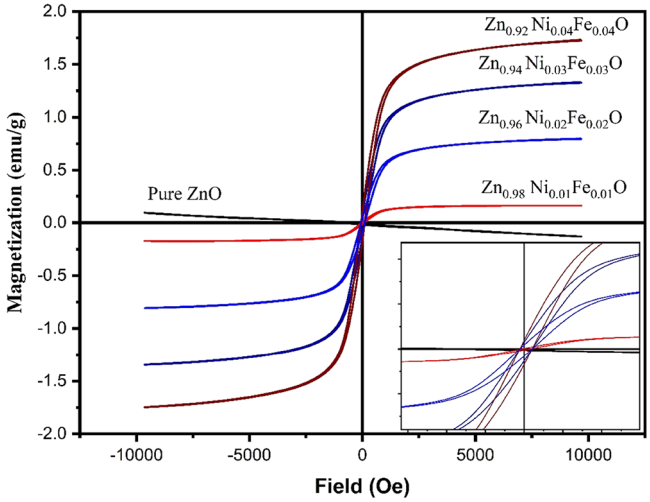

Figure 9. VSM results of ZnO, $Zn_{0.98}Ni_{0.01}Fe_{0.01}O$, $Zn_{0.968}Ni_{0.02}Fe_{0.02}O$, $Zn_{0.94}Ni_{0.03}Fe_{0.03}O$, and $Zn_{0.92}Ni_{0.04}Fe_{0.04}O$ NPs. The inset shows the zoomed-in view of $M-H$ loops of the samples.

pure and $Zn_{0.98}Ni_{0.01}Fe_{0.01}O$, $Zn_{0.968}Ni_{0.02}Fe_{0.02}O$, $Zn_{0.94}Ni_{0.03}Fe_{0.03}O$, and $Zn_{0.92}Ni_{0.04}Fe_{0.04}O$ samples measured at room temperature.

The $M-H$ curve of the pure ZnO sample showed diamagnetic nature of ZnO, which is due to the absence of intrinsic defects like zinc vacancies and oxygen vacancies, which is also investigated by many authors that undoped ZnO is diamagnetic even at very low temperatures.[43] The incorporation of Fe^{3+} and Ni^{2+} ions in the ZnO lattice is confirmed by the transformation of the diamagnetic behavior of the pure ZnO sample into the ferromagnetic nature of codoped samples. Room temperature ferromagnetism in doped ZnO NPs is due to various extrinsic and intrinsic phenomena. The extrinsic phenomenon occurs due to the formation of secondary phases or clusters of dopant semiconductor atoms and exchange interactions may occur under the intrinsic cause of magnetization.[44−46] The relationship between intrinsic defects due to oxygen or zinc vacancies and magnetism is also discussed in the literature.[46−51] From XRD analysis, it is also observed that the unit cell volume decreased with the increase in the doping concentrations as shown in Table 1,

https://doi.org/10.1021/acsomega.3c01727
ACS Omega 2024, 9, 137−145

which can also decrease the distance between dopant ions and strengthen the ferromagnetic ordering.[48,49] It is observed that magnetization increases with the applied magnetic field. The room temperature ferromagnetic behavior of doped (transition metals) NPs is recognized as the various intrinsic (exchange interaction) and extrinsic (the formation of clusters or secondary phases) phenomena by many authors.[45−51] The room temperature ferromagnetism in the doped samples is also attributed to the ferromagnetic coupling between magnetic ions (Ni^{2+} and Fe^{3+}) and oxygen vacancy associated with the bound magnetic polarons model.[16] The XRD results showed the successful addition of dopant ions to the wurtzite ZnO lattice. Since no secondary phase or clusters are observed in XRD spectra of Ni- and Fe-codoped ZnO samples, the observed ferromagnetism is an intrinsic property of synthesized doped ZnO NPs.

With an increase in doping concentration, the coercivity of samples was also improved, which represents the magnetic characteristics of the material. It is obvious from the XRD and UV−vis assimilation spectra investigation that Fe and Ni are effectively fused into the ZnO lattice; therefore, we have included the results of only three samples here. The beginning of attraction in the specimens is because of the exchange interactions between the spin-polarized electrons (for example, the electrons of Ni^{2+} and Fe^{2+} particles) and conductive electrons.[42−46] Hence, this can prompt the spin polarization of the conductive electrons. Therefore, all Ni^{2+} and Fe^{2+} ions display a similar turn bearing, bringing about the ferromagnetism of the material, after a progressive long-go exchange interaction.[48−52]

4. CONCLUSIONS

The present work demonstrates the fabrication and characterization of pure and Fe−Ni-codoped ZnO NPs using the sol−gel autocombustion route. Analysis of the samples was performed by using different diagnostic techniques. For instance, XRD confirmed that the hexagonal wurtzite structured NPs have been successfully fabricated. Due to lower values of ionic radii of iron and nickel, XRD peaks showed a redshift. SEM analysis supported the XRD results of hexagonal-shaped NPs. The crystallite size increased from 37 to 43 nm with an increase in the dopant concentration. The optical studies showed a decrease in the band gap from 3.20 to 3.13 eV for pure and doped ZnO NPs. Chemical compositions of the fabricated samples were confirmed using FTIR spectra. Finally, VSM measurements were performed to study the field-dependent magnetization. Field-dependent magnetization analysis was performed to observe the behavior of fabricated NPs; it was observed that pure ZnO showed diamagnetic, whereas doped ZnO NPs showed ferromagnetic behavior. By increasing the dopant concentrations, the magnetization of synthesized NPs showed an increasing trend. The room temperature ferromagnetism is attributed to the ferromagnetic coupling between magnetic ions (Ni^{2+} and Fe^{3+}) and oxygen vacancy associated with the bound magnetic polarons model. Current investigations demonstrated the fact that the ferromagnetic aspect perceived in the Ni- and Fe-codoped ZnO NPs is an intrinsic property. This work is useful for doping numerous transition metals in ZnO with extraordinary magnetic properties for various applications in spintronics. Also, further research studies can be carried out to inquire about electron- and hole-mediated ferromagnetism which offered valuable clues for the researchers working in the field of devices such as photonic crystals, detectors, and waveguides.

■ ASSOCIATED CONTENT

Data Availability Statement

All data have already been provided in the form of ORIGIN plots. Further requested data can be made available upon publisher's request.

■ AUTHOR INFORMATION

Corresponding Authors

Karwan Wasman Qadir − *Renewable Energy Technology Department, Erbil Technology College, Erbil Polytechnic University, Erbil, Kurdistan 44001, Iraq; Computation Nanotechnology Research Lab (CNRL), Department of Physics, College of Education, Salahaddin University-Erbil, Erbil, Kurdistan 44002, Iraq*; Email: karwanphysicist@gmail.com

Qayyum Zafar − *Department of Physics, University of Management and Technology, Lahore 54000, Pakistan*; orcid.org/0000-0001-6763-9587; Email: qayyumzafar@gmail.com

Authors

Nasar Ahmed − *Department of Physics, King Abdullah Campus, University of Azad Jammu and Kashmir, Muzaffarabad 13100, Pakistan*; orcid.org/0000-0003-0460-6571

Zakia Khalil − *Department of Physics, Mirpur University of Science and Technology, Muzaffarabad, Azad Jammu and Kashmir 10250, Pakistan*

Zahid Farooq − *Department of Physics, Division of Science and Technology, University of Education, Lahore 54000, Pakistan*

Khizar-ul-Haq − *Department of Physics, Mirpur University of Science and Technology, Muzaffarabad, Azad Jammu and Kashmir 10250, Pakistan*

Shabnam Shahida − *Department of Chemistry, University of Poonch, Rawalakot, Azad Kashmir 12350, Pakistan*

Ramiza − *Department of Physics, University of Agriculture, Faisalabad 38000, Pakistan*

Pervaiz Ahmad − *Department of Physics, King Abdullah Campus, University of Azad Jammu and Kashmir, Muzaffarabad 13100, Pakistan*

Rajwali Khan − *Department of Physics, University of Lakki Marwat, Lakki Marwat, Khyber Pakhtunkhwa 28440, Pakistan; Department of Physics, United Arab Emirates University, Al ain 15551, United Arab Emirates*

Complete contact information is available at: https://pubs.acs.org/10.1021/acsomega.3c01727

Notes

The authors declare no competing financial interest.
Neither there are potential risks and ethical issues involved in the current research nor authors have engaged in any form of malicious harm to another person or animal.

■ ACKNOWLEDGMENTS

The authors gratefully acknowledge the research facilities provided by the University of Azad Jammu and Kashmir.

https://doi.org/10.1021/acsomega.3c01727
ACS Omega 2024, 9, 137−145

REFERENCES

(1) Peter capper, S. O. K. Arthur Willoughby. In *Zinc oxide materials for electronic and optoelectronic device applications*; John Wiley & Sons, 2011.

(2) Sulciute, A.; Nishimura, K.; Gilshtein, E.; Cesano, F.; Viscardi, G.; Nasibulin, A. G.; Ohno, Y.; Rackauskas, S. ZnO Nanostructures Application in Electrochemistry: Influence of Morphology. *J. Phys. Chem. C* **2021**, *125* (2), 1472−1482.

(3) Lu, J.; Shi, Z.; Wang, Y.; Lin, Y.; Zhu, Q.; Tian, Z.; Dai, J.; Wang, S.; Xu, C. Plasmon-enhanced Electrically Light-emitting from ZnO Nanorod Arrays/p-GaN Heterostructure Devices. *Sci. Rep.* **2016**, *6* (1), 25645.

(4) Akram, R.; Almohaimeed, Z. M.; Bashir, A.; Ikram, M.; Qadir, K. W.; Zafar, Q. Synthesis and characterization of pristine and strontium-doped zinc oxide nanoparticles for methyl green photo-degradation application. *Nanotechnology* **2022**, *33* (29), 295702.

(5) Wang, Z. L.; Song, J. Piezoelectric nanogenerators based on zinc oxide nanowire arrays. *Science* **2006**, *312* (5771), 242−246.

(6) Al-ruqeishi, M. S.; Mohiuddin, T.; Al-habsi, B.; Al-ruqeishi, F.; Al-fahdi, A.; Al-khusaibi, A. Piezoelectric nanogenerator based on ZnO nanorods. *Arabian J. Chem.* **2019**, *12* (8), 5173−5179.

(7) Sutar, S. S.; Patil, S. M.; Kadam, S. J.; Kamat, R. K.; Kim, D.-K.; Dongale, T. D. Analysis and Prediction of Hydrothermally Synthesized ZnO-Based Dye-Sensitized Solar Cell Properties Using Statistical and Machine-Learning Techniques. *ACS Omega* **2021**, *6* (44), 29982−29992.

(8) Behera, M. K.; Williams, L. C.; Pradhan, S. K.; Bahoura, M. Reduced Transition Temperature in Al:ZnO/VO_2 Based Multi-Layered Device for low Powered Smart Window Application. *Sci. Rep.* **2020**, *10* (1), 1824.

(9) Jiang, L.; Li, J.; Huang, K.; Li, S.; Wang, Q.; Sun, Z.; Mei, T.; Wang, J.; Zhang, L.; Wang, N. Low-Temperature and Solution-Processable Zinc Oxide Transistors for Transparent Electronics. *ACS Omega* **2017**, *2* (12), 8990−8996.

(10) Tsai, Y.-T.; Chang, S.-J.; Ji, L.-W.; Hsiao, Y.-J.; Tang, I. T.; Lu, H.-Y.; Chu, Y.-L. High Sensitivity of NO Gas Sensors Based on Novel Ag-Doped ZnO Nanoflowers Enhanced with a UV Light-Emitting Diode. *ACS Omega* **2018**, *3* (10), 13798−13807.

(11) Gharpure, S.; Yadwade, R.; Ankamwar, B. Non-antimicrobial and Non-anticancer Properties of ZnO Nanoparticles Biosynthesized Using Different Plant Parts of Bixa orellana. *ACS Omega* **2022**, *7* (2), 1914−1933.

(12) Ahmed, N.; Majid, A.; Khan, M. A.; Rashid, M.; Umar, Z. A.; Baig, M. A. Synthesis and characterization of Zn/ZnO microspheres on indented sites of silicon substrate. *Mater. Sci.* **2018**, *36* (3), 501−508.

(13) Sarfraz, M.; Ahmed, N.; Khizar ul, H.; Shahida, S.; Khan, M. A. Structural optical and magnetic properties of transition metal doped ZnO magnetic nanoparticles synthesized by sol-gel auto-combustion method. *Mater. Sci.* **2019**, *37* (2), 280−288.

(14) Faisal, S.; Jan, H.; Shah, S. A.; Shah, S.; Khan, A.; Akbar, M. T.; Rizwan, M.; Jan, F.; Wajidullah; Akhtar, N.; et al. Green Synthesis of Zinc Oxide (ZnO) Nanoparticles Using Aqueous Fruit Extracts of Myristica fragrans: Their Characterizations and Biological and Environmental Applications. *ACS Omega* **2021**, *6* (14), 9709−9722.

(15) Reuge, N.; Bacsa, R.; Serp, P.; Caussat, B. Chemical Vapor Synthesis of Zinc Oxide Nanoparticles: Experimental and Preliminary Modeling Studies. *J. Phys. Chem. C* **2009**, *113* (46), 19845−19852.

(16) Kanwal, S.; Khan, M. T.; Mehboob, N.; Amami, M.; Zaman, A. Room-Temperature Ferromagnetism in Cu/Co Co-Doped ZnO Nanoparticles Prepared by the Co-Precipitation Method: For Spintronics Applications. *ACS Omega* **2022**, *7* (36), 32184−32193.

(17) Lu, J. J.; Lin, T. C.; Tsai, S. Y.; Mo, T. S.; Gan, K. J. Structural, magnetic and transport properties of Ni-doped ZnO films. *J. Magn. Magn. Mater.* **2011**, *323* (6), 829−832.

(18) Tanaka, M.; Higo, Y. Large Tunneling Magnetoresistance in GaMnAs/AlAs/GaMnAs Ferromagnetic Semiconductor Tunnel Junctions. *Phys. Rev. Lett.* **2001**, *87* (2), No. 026602.

(19) Pearton, S. J.; Abernathy, C. R.; Overberg, M. E.; Thaler, G. T.; Norton, D. P.; Theodoropoulou, N.; Hebard, A. F.; Park, Y. D.; Ren, F.; Kim, J. Wide band gap ferromagnetic semiconductors and oxides. *J. Appl. Phys.* **2003**, *93* (1), 1−13.

(20) Wang, Y. X.; Liu, H.; Li, Z. Q.; Zhang, X. X.; Zheng, R. K.; Ringer, S. P. Role of structural defects on ferromagnetism in amorphous Cr-doped TiO_2 films. *Appl. Phys. Lett.* **2006**, *89* (4), No. 042511.

(21) Dietl, T.; Ohno, H.; Matsukura, F. Hole-mediated ferromagnetism in tetrahedrally coordinated semiconductors. *Phys. Rev. B* **2001**, *63* (19), No. 195205.

(22) Mandal, S. K.; Das, A. K.; Nath, T. K.; Karmakar, D. Temperature dependence of solubility limits of transition metals (Co, Mn, Fe, and Ni) in ZnO nanoparticles. *Appl. Phys. Lett.* **2006**, *89* (14), 144105.

(23) Birajdar, S. D.; Khirade, P. P.; Bhagwat, V. R.; Humbe, A. V.; Jadhav, K. M. Synthesis, structural, morphological, optical and magnetic properties of $Zn_{1-x}Co_xO$ ($0 \leq x \leq 0.36$) nanoparticles synthesized by sol-gel auto combustion method. *J. Alloys Compd.* **2016**, *683*, 513−526.

(24) Avrutin, V.; Izyumskaya, N.; Ü, O.; Silversmith, D. J.; Morkoç, H. Ferromagnetism in ZnO- and GaN-Based Diluted Magnetic Semiconductors: Achievements and Challenges. *Proc. IEEE* **2010**, *98* (7), 1288−1301.

(25) Aruna, S. T.; Mukasyan, A. S. Combustion synthesis and nanomaterials. *Curr. Opin. Solid State Mater. Sci.* **2008**, *12* (3), 44−50.

(26) Anbuselvan, D.; Nilavazhagan, S.; Santhanam, A.; Chidhambaram, N.; Gunavathy, K. V.; Ahamad, T.; Alshehri, S. M. Room temperature ferromagnetic behavior of nickel-doped zinc oxide dilute magnetic semiconductor for spintronics applications. *Phys. E* **2021**, *129*, No. 114665.

(27) Chang, G. S.; Kurmaev, E. Z.; Boukhvalov, D. W.; Finkelstein, L. D.; Moewes, A.; Bieber, H.; Colis, S.; Dinia, A.; et al. *J. Phys.: Condens. Matter* **2009**, *21* (5), No. 056002.

(28) Laiho, R.; Ojala, I.; Vlasenko, L. Percolation of ferromagnetism in ZnO codoped with Fe and Mg. *J. Appl. Phys.* **2010**, *108* (5), No. 053915.

(29) Zhong, M.; Li, Y.; Tariq, M.; Hu, Y.; Li, W.; Zhu, M.; Jin, H.; Li, Y. Effect of oxygen vacancy induced by pulsed magnetic field on the room-temperature ferromagnetic Ni-doped ZnO synthesized by hydrothermal method. *J. Alloys Compd.* **2016**, *675*, 286−291.

(30) Wu, X.; Wei, Z.; Zhang, L.; Zhang, C.; Yang, H.; Jiang, J. Synthesis and characterization of Fe and Ni co-doped ZnO nanorods synthesized by a hydrothermal method. *Ceram. Int.* **2014**, *40* (9, Part B), 14635−14640.

(31) Prabakar, C.; Muthukumaran, S.; Raja, V. Structural, magnetic and photoluminescence behavior of Ni/Fe doped ZnO nanostructures prepared by co-precipitation method. *Optik* **2020**, *202*, No. 163714.

(32) Farias, A. F. F.; De araújo, D. T.; Da silva, A. L.; Leal, E.; Pacheco, J. G. A.; Silva, M. R.; Kiminami, R. H. G. A.; Costa, A. C. F. D. M. Evaluation of the catalytic effect of ZnO as a secondary phase in the $Ni_{0.5}Zn_{0.5}Fe_2O_4$ system and of the stirring mechanism on biodiesel production reaction. *Arabian J. Chem.* **2020**, *13* (6), 5788−5799.

(33) Tong, L.-N.; Cheng, T.; Han, H.-B.; Hu, J.-L.; He, X.-M.; Tong, Y.; Schneider, C. M. Photoluminescence studies on structural defects and room temperature ferromagnetism in Ni and Ni−H doped ZnO nanoparticles. *J. Appl. Phys.* **2010**, *108* (2), No. 023906.

(34) Wang, L. M.; Liao, J.-W.; Peng, Z.-A.; Lai, J.-H. Doping Effects on the Characteristics of Fe:ZnO Films: Valence Transition and Hopping Transport. *J. Electrochem. Soc.* **2009**, *156* (2), H138.

(35) Akram, R.; Fatima, A.; Almohaimeed, Z. M.; Farooq, Z.; Qadir, K. W.; Zafar, Q. Photocatalytic Degradation of Methyl Green Dye Mediated by Pure and Mn-Doped Zinc Oxide Nanoparticles under Solar Light Irradiation. *Adsorpt. Sci. Technol.* **2023**, *2023*, No. 5069872.

(36) Zak, A. K.; Abrishami, M. E.; Majid, W. H. A.; Yousefi, R.; Hosseini, S. M. Effects of annealing temperature on some structural

https://doi.org/10.1021/acsomega.3c01727
ACS Omega 2024, 9, 137−145

and optical properties of ZnO nanoparticles prepared by a modified sol−gel combustion method. *Ceram. Int.* **2011**, *37* (1), 393−398.
(37) Yousefi, R.; Zak, A. K.; Jamali-sheini, F. The effect of group-I elements on the structural and optical properties of ZnO nanoparticles. *Ceram. Int.* **2013**, *39* (2), 1371−1377.
(38) Yadav, M. K.; Ghosh, M.; Biswas, R.; Raychaudhuri, A. K.; Mookerjee, A.; Datta, S. Band-gap variation in Mg- and Cd-doped ZnO nanostructures and molecular clusters. *Phys. Rev. B* **2007**, *76* (19), No. 195450.
(39) Wu, X.; Wei, Z.; Zhang, L.; Wang, X.; Yang, H.; Jiang, J. Optical and magnetic properties of Fe doped ZnO nanoparticles obtained by hydrothermal synthesis. *J. Nanomater.* **2014**, *2014*, No. 792102.
(40) Dhiman, P.; Chand, J.; Kumar, A.; Kotnala, R. K.; Batoo, K. M.; Singh, M. Synthesis and characterization of novel Fe@ZnO nanosystem. *J. Alloys Compd.* **2013**, *578*, 235−241.
(41) Moss, T. S. A Relationship between the Refractive Index and the Infra-Red Threshold of Sensitivity for Photoconductors. *Proc. Phys. Soc. London, Sect. B* **1950**, *63* (3), 167.
(42) Ravindra, N. M.; Ganapathy, P.; Choi, J. Energy gap−refractive index relations in semiconductors − An overview. *Infrared Phys. Technol.* **2007**, *50* (1), 21−29.
(43) Muth, J.; Osinsky, A. Optical Properties of ZnO Alloys. In *Wide Bandgap Light Emitting Materials and Devices*; 2007; pp 179−204.
(44) Aydın, H.; Aydın, C.; Al-ghamdi, A. A.; Farooq, W. A.; Yakuphanoglu, F. Refractive index dispersion properties of Cr-doped ZnO thin films by sol−gel spin coating method. *Optik* **2016**, *127* (4), 1879−1883.
(45) Paskaleva, A.; Buchkov, K.; Galluzzi, A.; Spassov, D.; Blagoev, B.; Ivanov, T.; Mehandzhiev, V.; Avramova, I. A.; Terzyiska, P.; Tzvetkov, P.; et al. Magneto-Optical and Muliferroic Properties of Transition-Metal (Fe, Co, or Ni)-Doped ZnO Layers Deposited by ALD. *ACS Omega* **2022**, *7* (47), 43306−43315.
(46) Potzger, K.; Zhou, S.; Eichhorn, F.; Helm, M.; Skorupa, W.; Mücklich, A.; Fassbender, J.; Herrmannsdörfer, T.; Bianchi, A. Ferromagnetic Gd-implanted ZnO single crystals. *J. Appl. Phys.* **2006**, *99* (6), No. 063906.
(47) Birajdar, S. D.; Khirade, P. P.; Humbe, A. V.; Jadhav, K. M. Presence of intrinsic defects and transition from diamagnetic to ferromagnetic state in Co2 + ions doped ZnO nanoparticles. *J. Mater. Sci.: Mater. Electron.* **2016**, *27* (6), 5575−5583.
(48) Sharma, R. K.; Patel, S.; Pargaien, K. C. Synthesis, characterization and properties of Mn-doped ZnO nanocrystals. *Adv. Nat. Sci.: Nanosci. Nanotechnol.* **2012**, *3* (3), No. 035005.
(49) Liu, F.; Grundke-iqbal, I.; Iqbal, K.; Gong, C.-X. Contributions of protein phosphatases PP1, PP2A, PP2B and PP5 to the regulation of tau phosphorylation. *Eur. J. Neurosci.* **2005**, *22* (8), 1942−1950.
(50) Pal, B.; Giri, P. K. Defect Mediated Magnetic Interaction and High T c Ferromagnetism in Co Doped ZnO Nanoparticles. *J. Nanosci. Nanotechnol.* **2011**, *11* (10), 9167−9174.
(51) Santara, B.; Giri, P. K.; Dhara, S.; Imakita, K.; Fujii, M. Oxygen vacancy-mediated enhanced ferromagnetism in undoped and Fe-doped TiO2 nanoribbons. *J. Phys. D: Appl. Phys.* **2014**, *47* (23), No. 235304.
(52) Coey, J. M. D.; Venkatesan, M.; Fitzgerald, C. B. Donor impurity band exchange in dilute ferromagnetic oxides. *Nat. Mater.* **2005**, *4* (2), 173−179.

https://doi.org/10.1021/acsomega.3c01727
ACS Omega 2024, 9, 137−145